Draft version June 3, 2020
Typeset using LaTeX default style in AASTeX61



# A CATALOG OF HOLES AND SHELLS IN THE INTERSTELLAR MEDIUM OF THE LITTLE THINGS DWARF GALAXIES

Nau Raj Pokhrel,[1,2] Caroline E. Simpson,[1] and Ioannis Bagetakos[3]

[1] *Department of Physics, Florida International University, 11200 SW 8th St., Miami, FL 33199, USA*
[2] *Department of Physics and Astronomy, The University of Tennessee, 1408 Circle Drive, Knoxville, TN 37996, USA*
[3] *ASTRON, the Netherlands Institute for Radio Astronomy, Postbus 2, 7990 AA, Dwingeloo, The Netherlands*

## ABSTRACT

We present a catalog of holes and shells in the neutral atomic hydrogen (H I) of 41 gas-rich dwarf galaxies in LITTLE THINGS (Local Irregulars That Trace Luminosity Extremes, The H I Nearby Galaxy Survey). We analyzed their properties as part of an investigation into the relation between star formation and structures and kinematics in the H I of small galaxies. We confirmed 306 holes between 38 pc (our resolution limit) and 2.3 kpc, with expansion velocities up to 30 km $s^{-1}$. The global star formation rates measured by H$\alpha$ and FUV emission are consistent with those estimated from the energy required to create the cataloged holes in our sample. Although we found no obvious correlation between global star-formation rates and the H I surface and volume porosities of our sample, two of the four lowest porosity galaxies and the two highest porosity galaxies have no recent star formation as measured by H$\alpha$ and FUV emission.

**Table 1.** Basic Galaxy Information

| Galaxy | RA (J2000) | Dec (J2000) | Distance [a] | PA[a] | Inclination[a] | $R_D$ [b] |
|---|---|---|---|---|---|---|
| | (hh mm ss.s) | (dd mm ss) | (Mpc) | (deg) | (deg) | (kpc) |
| CVnIdwA | 12 38 40.2 | +32 45 40 | 3.6 | 80 | 41.0 | 0.57 |
| DDO 43 | 07 28 17.8 | +40 46 13 | 7.8 | 6.5 | 48.5 | 0.41 |
| DDO 46 | 07 41 26.6 | +40 06 39 | 6.1 | 84 | 28.6 | 1.14 |
| DDO 47 | 07 41 55.3 | +16 48 08 | 5.2 | −70 | 64.4 | 1.36 |
| DDO 50 | 08 19 08.7 | +70 43 25 | 3.4 | 18 | 46.7 | 1.10 |
| DDO 52 | 08 28 28.5 | +41 51 21 | 10.3 | 5 | 51.1 | 1.32 |
| DDO 53 | 08 34 08.0 | +66 10 37 | 3.6 | 81 | 64.4 | 0.72 |
| DDO 63 | 09 40 30.4 | +71 11 02 | 3.9 | 0 | 0 | 0.68 |
| DDO 69 | 09 59 25.0 | +30 44 42 | 0.8 | −64 | 60.3 | 0.19 |
| DDO 70 | 10 00 00.9 | +05 19 50 | 1.3 | 88 | 57.8 | 0.48 |
| DDO 75 | 10 10 59.2 | −04 41 56 | 1.3 | 41 | 33.5 | 0.22 |
| DDO 87 | 10 49 34.7 | +65 31 46 | 7.7 | 76.5 | 58.6 | 1.31 |
| DDO 101 | 11 55 39.4 | +31 31 08 | 6.4 | −69 | 49.4 | 0.93 |
| DDO 126 | 12 27 06.5 | +37 08 23 | 4.9 | −41 | 67.7 | 0.87 |
| DDO 133 | 12 32 55.4 | +31 32 14 | 3.5 | −6 | 49.4 | 1.24 |
| DDO 154 | 12 54 06.2 | +27 09 02 | 3.7 | 46 | 65.2 | 0.59 |
| DDO 155 | 12 58 39.8 | +14 13 10 | 2.2 | 51 | 47.6 | 0.15 |
| DDO 165 | 13 06 25.3 | +67 42 25 | 4.6 | 89 | 61.9 | 2.26 |
| DDO 167 | 13 13 22.9 | +46 19 11 | 4.2 | −23 | 52.8 | 0.33 |
| DDO 168 | 13 14 27.2 | +45 55 46 | 4.3 | −24.5 | 54.5 | 0.83 |
| DDO 187 | 14 15 56.7 | +23 03 19 | 2.2 | 37 | 39.0 | 0.18 |
| DDO 210 | 20 46 52.0 | −12 50 50 | 0.9 | −85 | 66.9 | 0.17 |
| DDO 216 | 23 28 35.0 | +14 44 30 | 1.1 | −58 | 69.4 | 0.54 |
| F564-V3 | 09 02 53.9 | +20 04 29 | 8.7 | 7 | 35.8 | 0.53 |
| Haro 29 | 12 26 16.7 | +48 29 38 | 5.8 | 85 | 58.6 | 0.29 |
| Haro 36 | 12 46 56.3 | +51 36 48 | 9.3 | 2 | 37.9 | 0.68 |
| IC 10 | 00 20 21.9 | +59 17 39 | 0.7 | −38 | 41.0 | 0.40 |
| IC 1613 | 01 04 49.2 | +02 07 48 | 0.7 | 71 | 37.9 | 0.58 |
| LGS 3 | 01 03 55.2 | +21 52 39 | 0.7 | −3.5 | 64.4 | 0.23 |
| M81dwA | 08 23 57.2 | +71 01 51 | 3.5 | 86 | 45.8 | 0.25 |
| Mrk 178 | 11 33 29.0 | +49 14 24 | 3.9 | −50 | 68.6 | 0.33 |
| NGC 1569 | 04 30 49.8 | +64 50 51 | 3.4 | −59 | 61.1 | 0.39 |
| NGC 2366 | 07 28 48.8 | +69 12 22 | 3.4 | 32.5 | 72.1 | 1.35 |
| NGC 3738 | 11 35 49.0 | +54 31 23 | 4.9 | 0 | 0 | 0.78 |
| NGC 4163 | 12 12 09.2 | +36 10 13 | 2.9 | 18 | 53.7 | 0.27 |
| NGC 4214 | 12 15 39.2 | +36 19 38 | 3.0 | 16 | 25.8 | 0.75 |
| NGC 6822 | 19 44 57.9 | −14 48 11 | 0.5 | 24 | ··· | 0.57 |
| SagDIG | 19 30 00.6 | −17 40 56 | 1.1 | 87.5 | 62.7 | 0.23 |
| UGC 8508 | 13 30 44.9 | +54 54 29 | 2.6 | −60 | 61.9 | 0.26 |
| WLM | 00 01 59.2 | −15 27 41 | 1.0 | −2 | 70.3 | 0.57 |
| VIIZw 403 | 11 27 58.2 | +78 59 39 | 4.4 | −10 | 66.0 | 0.52 |

[a] Hunter et al. (2012)

[b] V-band scale length from Hunter & Elmegreen (2004)

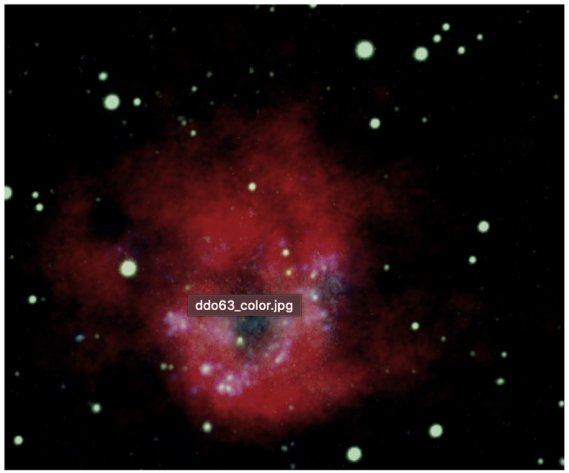


The Astronomical Journal, 141:23 (35pp), 2011 January doi:10.1088/0004-6256/141/1/23


# THE FINE-SCALE STRUCTURE OF THE NEUTRAL INTERSTELLAR MEDIUM IN NEARBY GALAXIES

I. Bagetakos[1], E. Brinks[1], F. Walter[2], W. J. G. de Blok[3], A. Usero[4], A. K. Leroy[2,5,8], J. W. Rich[6], and R. C. Kennicutt, Jr.[7]

[1] Centre for Astrophysics Research, Science & Technology Research Institute, University of Hertfordshire, Hatfield AL10 9AB, UK; i.bagetakos@herts.ac.uk, e.brinks@herts.ac.uk
[2] Max-Planck-Institut für Astronomie, Königstuhl 17, 69117 Heidelberg, Germany; walter@mpia-hd.mpg.de, aleroy@nrao.edu
[3] Department of Astronomy, University of Cape Town, Private Bag X3, Rondebosch 7701, South Africa; edeblok@ast.uct.ac.za
[4] Observatorio Astronómico Nacional, C/Alfonso XII 3, Madrid 28014, Spain; a.usero@oan.es
[5] National Radio Astronomy Observatory, 520 Edgemont Road, Charlottesville, VA 22903, USA
[6] Research School of Astronomy & Astrophysics, ANU, Mount Stromlo Observatory, Cotter Road, Weston Creek, ACT 2611, Australia; joshua@mso.anu.edu.au
[7] Institute of Astronomy, University of Cambridge, Madingley Road, Cambridge CB3 0HA, UK; robk@ast.cam.ac.uk

*Received 2010 April 19; accepted 2010 August 6; published 2010 December 10*

## ABSTRACT

We present an analysis of the properties of H I holes detected in 20 galaxies that are part of "The H I Nearby Galaxy Survey." We detected more than 1000 holes in total in the sampled galaxies. Where they can be measured, their sizes range from about 100 pc (our resolution limit) to about 2 kpc, their expansion velocities range from 4 to 36 km s$^{-1}$, and their ages are estimated to range between 3 and 150 Myr. The holes are found throughout the disks of the galaxies, out to the edge of the H I disk; 23% of the holes fall outside $R_{25}$. We find that shear limits the age of holes in spirals (shear is less important in dwarf galaxies) which explains why H I holes in dwarfs are rounder, on average than in spirals. Shear, which is particularly strong in the inner part of spiral galaxies, also explains why we find that holes outside $R_{25}$ are larger and older. We derive the scale height of the H I disk as a function of galactocentric radius and find that the disk flares up in all galaxies. We proceed to derive the surface and volume porosity ($Q_{2D}$ and $Q_{3D}$) and find that this correlates with the type of the host galaxy: later Hubble types tend to be more porous. The size distribution of the holes in our sample follows a power law with a slope of $a_\nu \sim -2.9$. Assuming that the holes are the result of massive star formation (SF), we derive values for the supernova rate and star formation rate (SFR) which scales with the SFR derived based on other tracers. If we extrapolate the observed number of holes to include those that fall below our resolution limit, down to holes created by a single supernova, we find that our results are compatible with the hypothesis that H I holes result from SF.

*Key words:* galaxies: ISM – galaxies: structure – ISM: bubbles – ISM: structure

*Online-only material:* color figure, figure set, machine-readable and VO tables

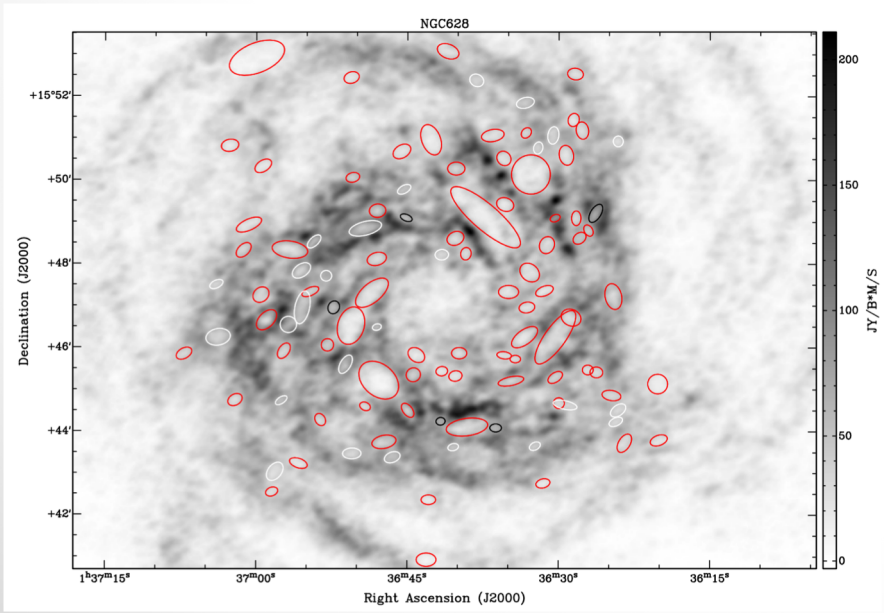


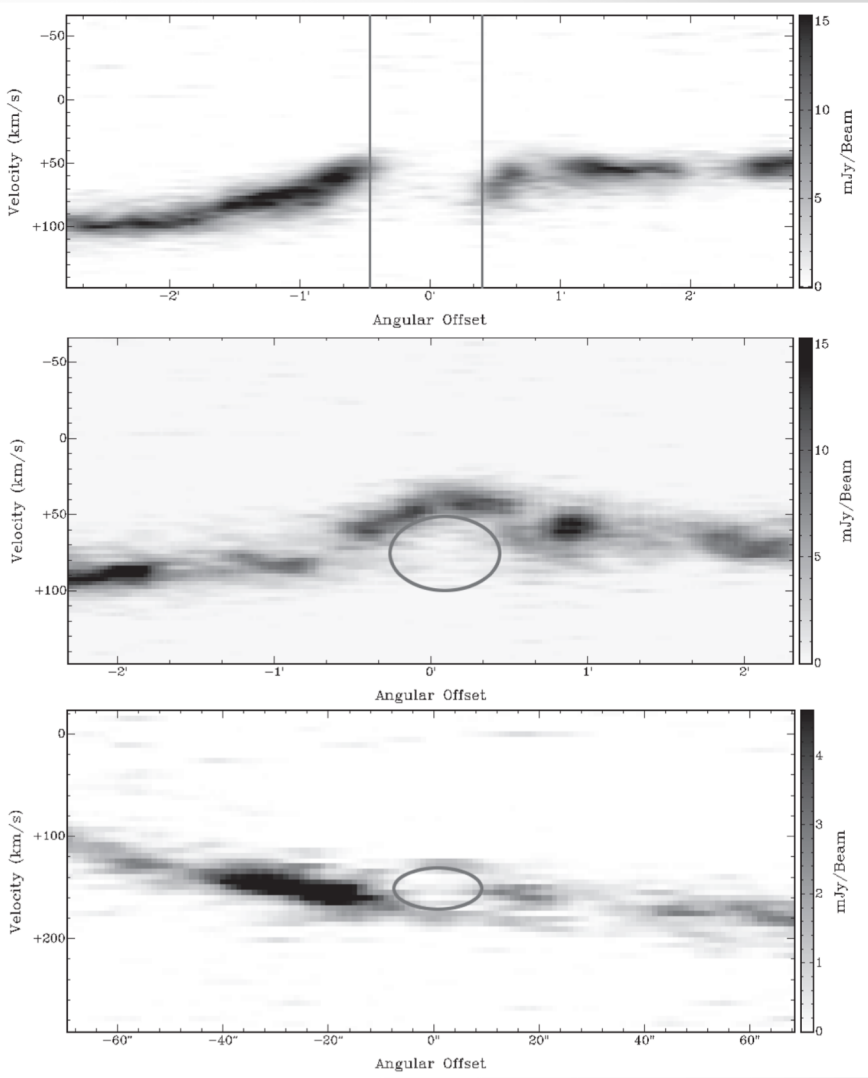

Используемый ими подход:

1) Используя пакет KARMA, визуально ищут кандидаты в полости HI на интегральных картах HI (нашли 1181)
2) Смотрят на «мультик» из поканальных изображений, чтобы проверить, что полости видны хотя бы в нескольких каналах
3) Строят PV-диаграммы, чтобы увидеть признаки расширения оболочки, определить скорость расширения и провести классификацию

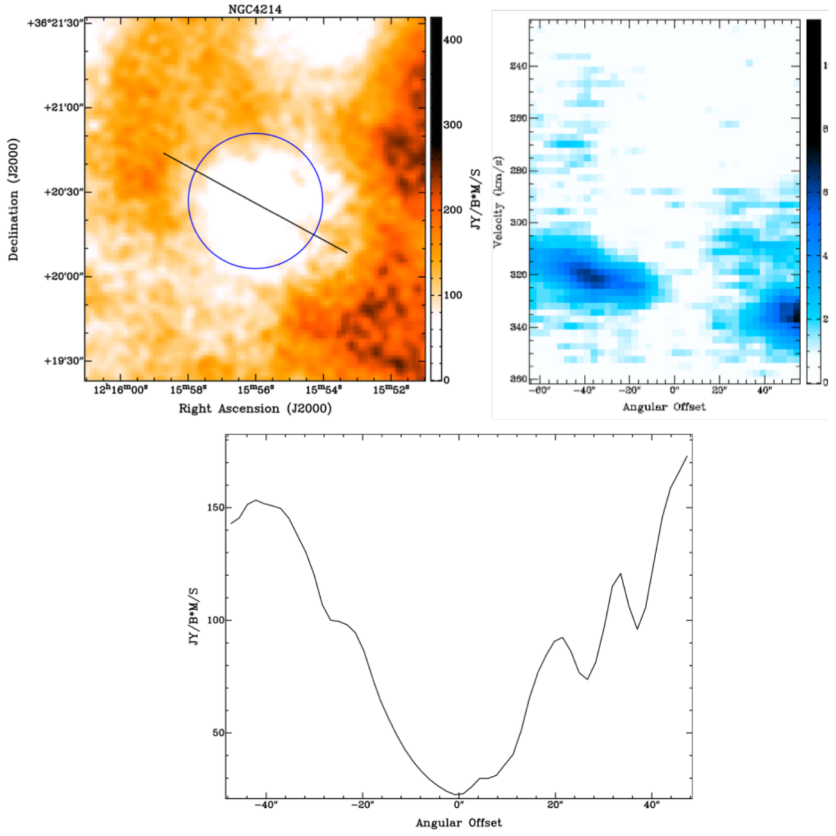


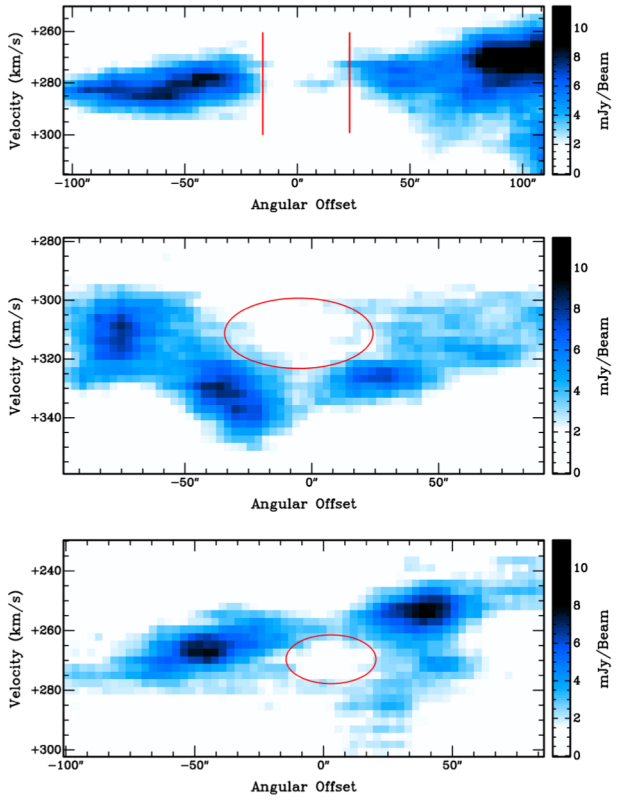


**Figure 2.** Position-velocity ($pv$) diagrams of three types of holes (these features are from NGC 4214). Top: Type 1 hole (completely blown out); middle: Type 2 hole (partially blown out); and bottom: Type 3 hole (intact).

$$E_{\rm Ch}\,({\rm erg}) = 5.3\times10^{43}\,n_0^{1.12}\,({\rm cm^{-3}})\left(\frac{d\,({\rm pc})}{2}\right)^{3.12} v_{\rm exp}^{1.4}\,({\rm km\,s^{-1}}).$$

Chevalier+ (1974)

$$E_{\rm Mc}\,({\rm erg}) = n_0\left(\frac{d\,({\rm pc})}{194}\right)^2\left(\frac{v_{\rm exp}\,({\rm km\,s^{-1}})}{5.7}\right)^3\times10^{51}.$$

McCray & Kafatos (1987)

$$t_{\rm kin} = 0.978\,\frac{d/2}{v_{\rm exp}}$$

Почему не t=0.3R/v *или* t=0.6R/v ?

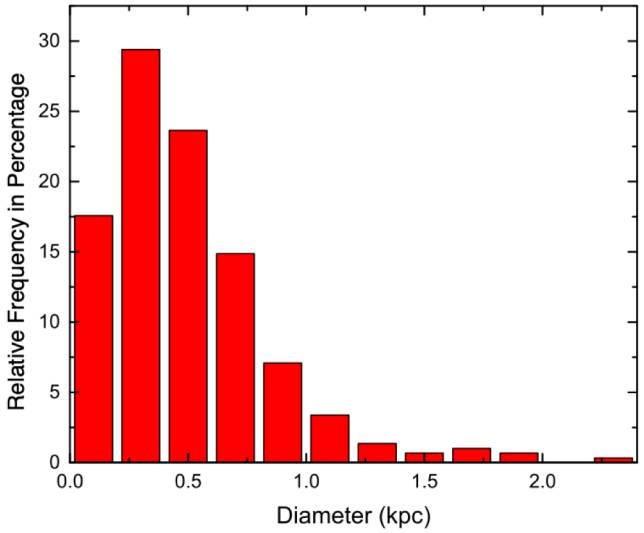


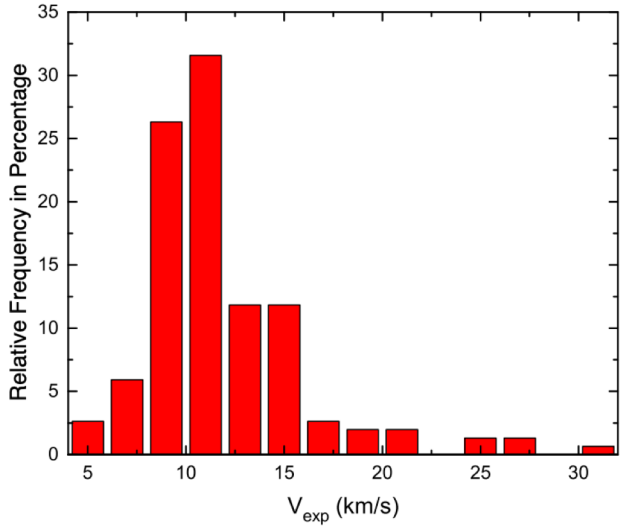


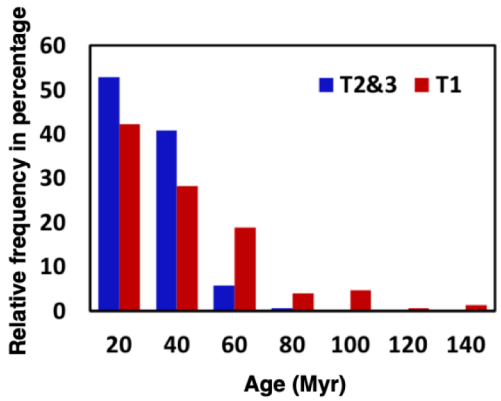

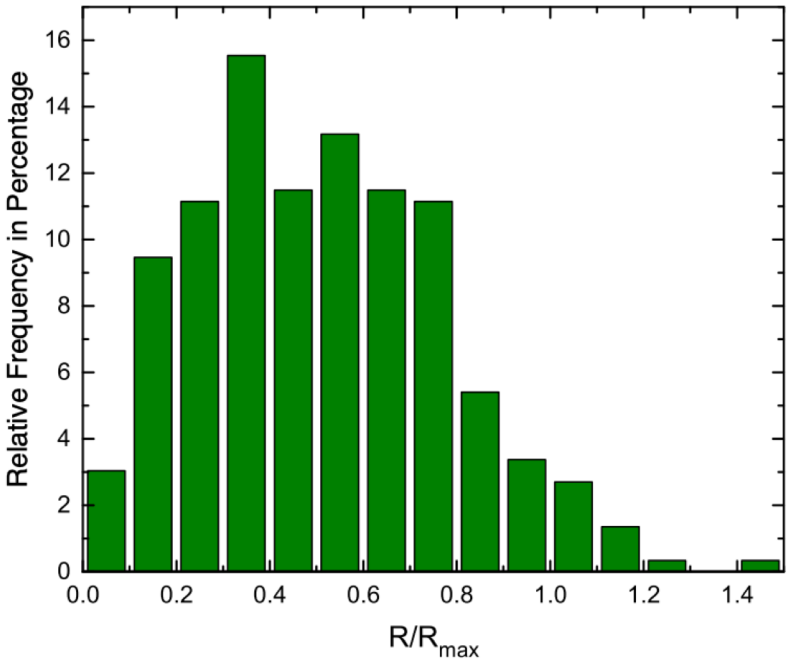


Около 85% оболочек наблюдается внутри интервала (0.15-0.8) Rmax

DDO 63, DDO 154, NGC 2366, NGC 4214
IC 1613 – оболочки в центральной части галактики…

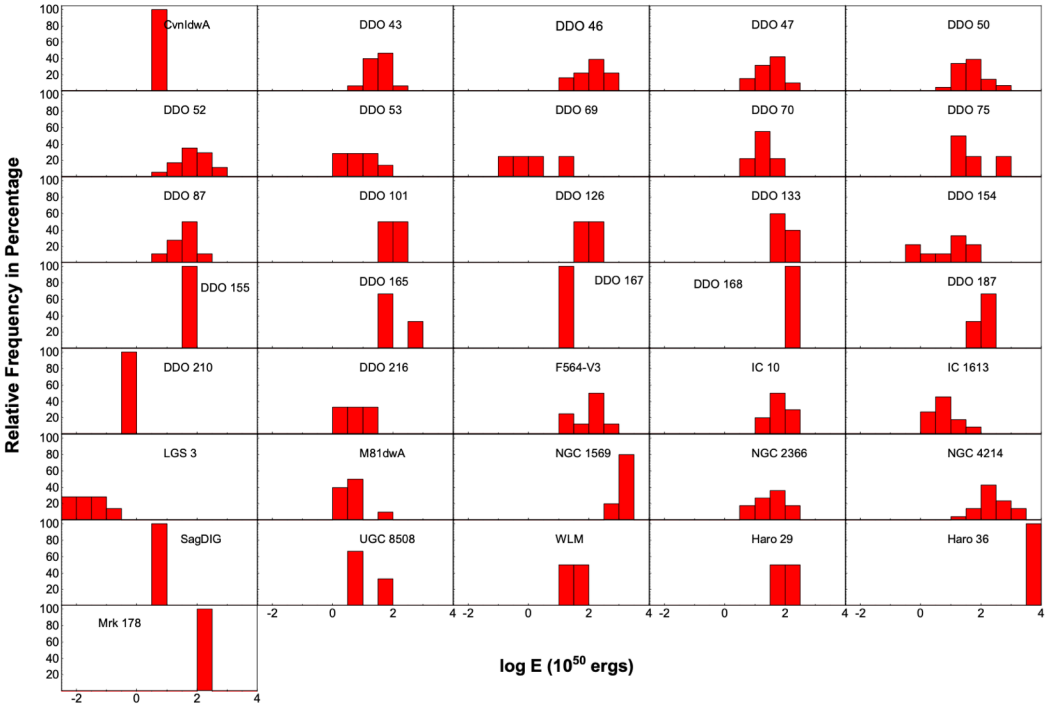


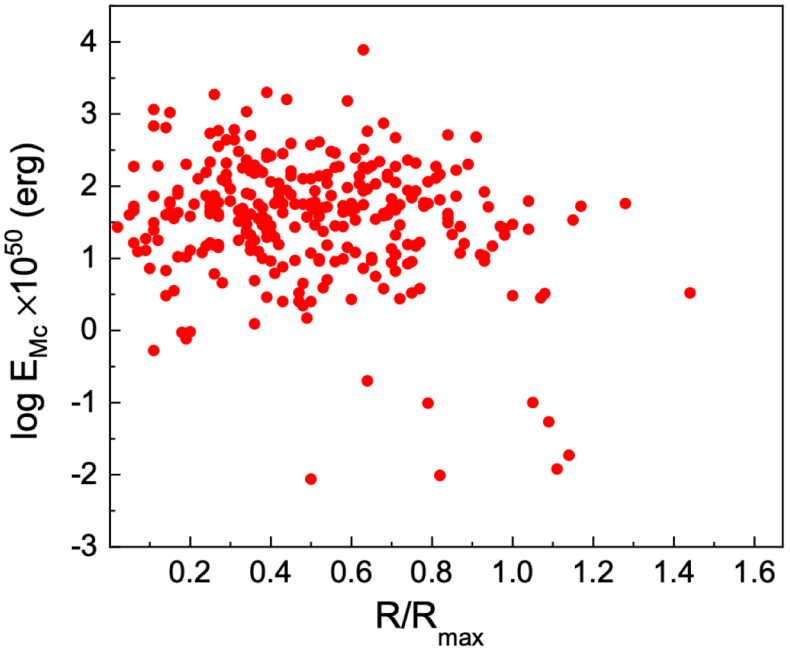

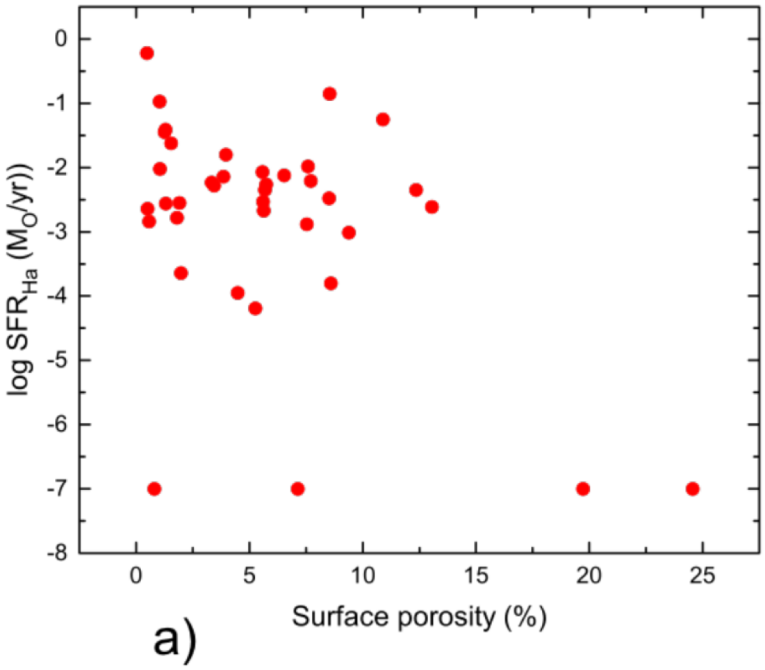
log SFR$_{Ha}$ ($M_O$/yr))
Surface porosity (%)
a)

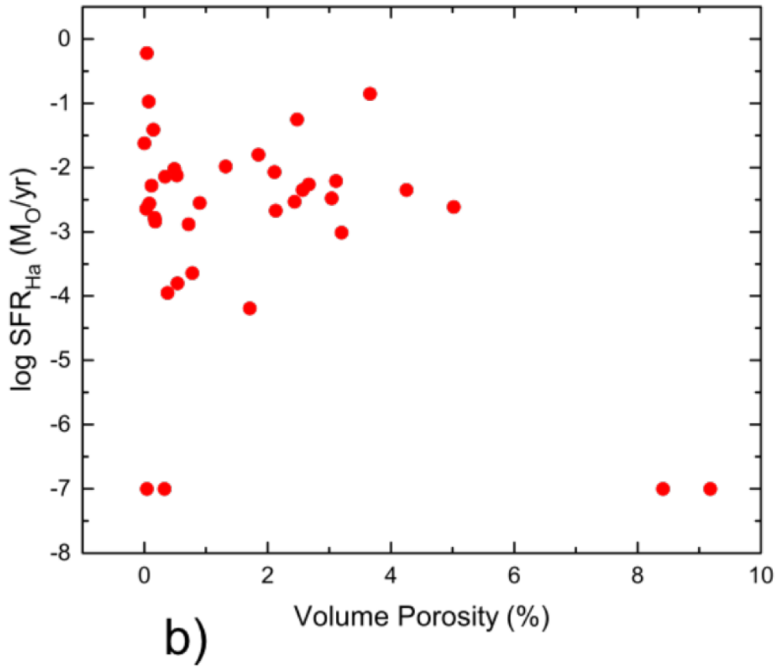
log SFR$_{Ha}$ ($M_O$/yr)
Volume Porosity (%)
b)

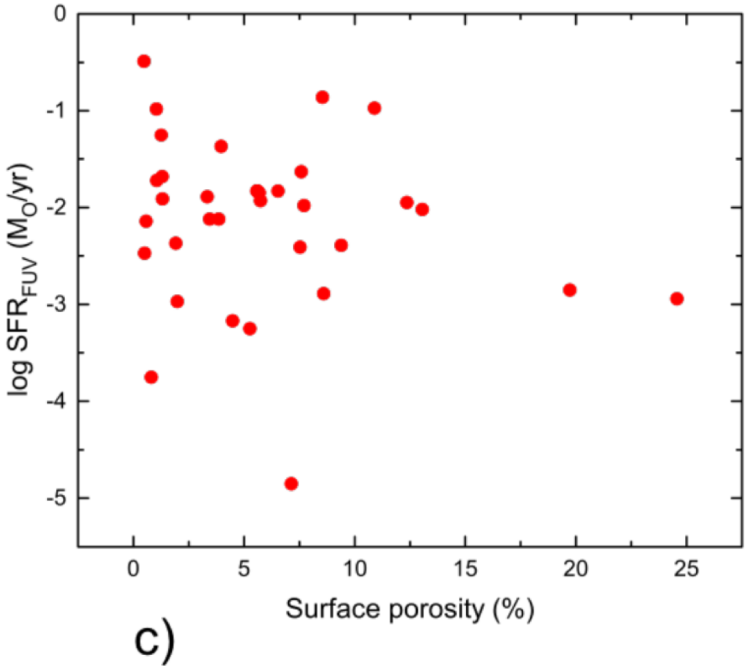
log SFR$_{FUV}$ ($M_O$/yr)
Surface porosity (%)
c)

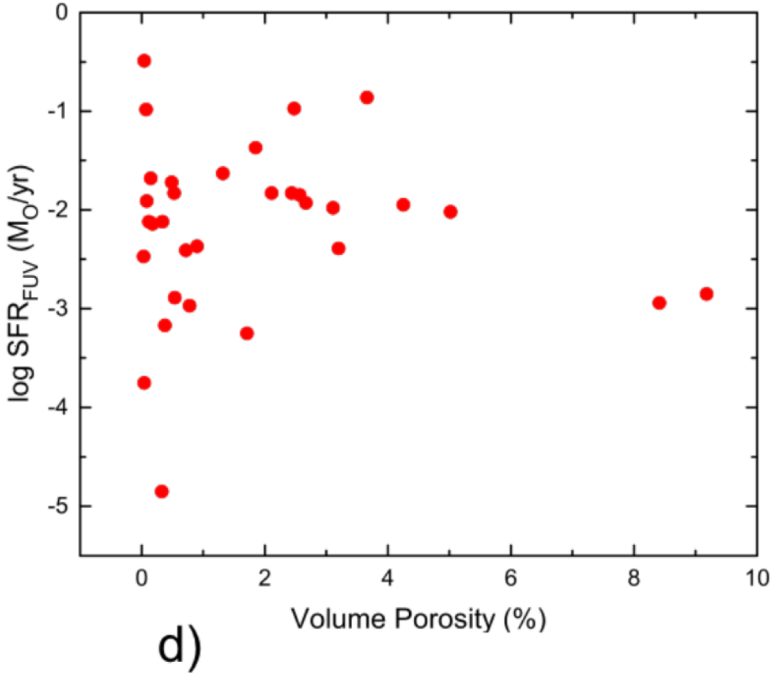
log SFR$_{FUV}$ ($M_O$/yr)
Volume Porosity (%)
d)

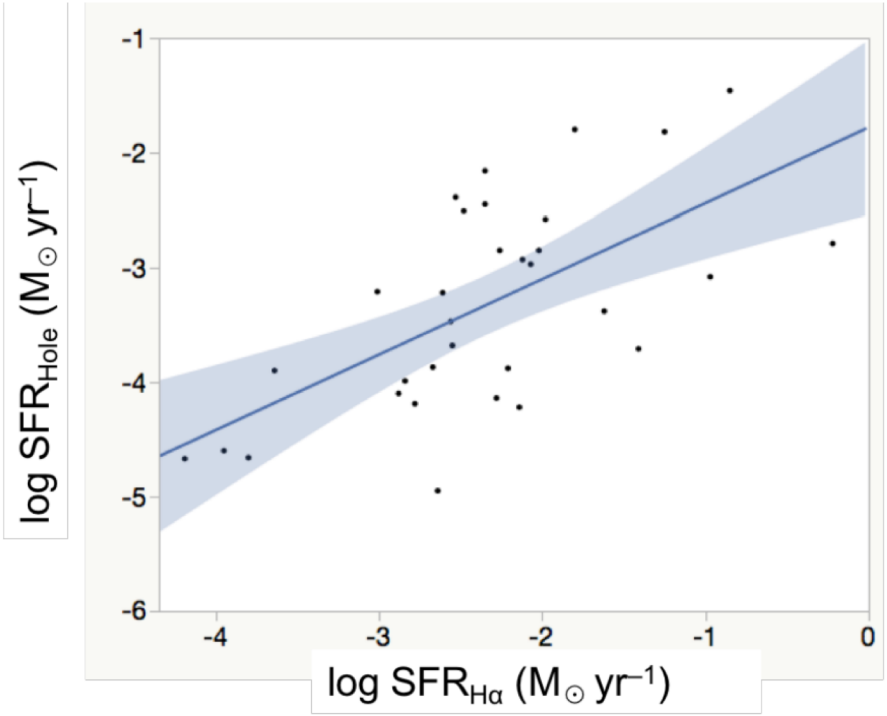


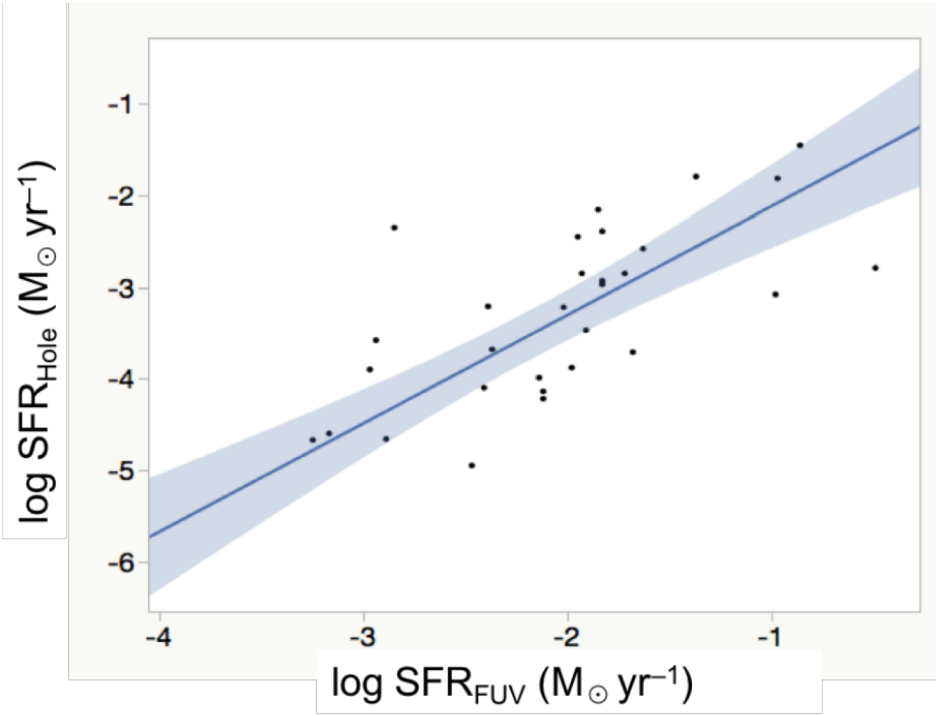


Оценивают SFR из энергии оболочек E_ch, пересчитанной в число сверхновых, IMF (Salpeter), возраста оболочек t~60 Myr (почему не 40?)

$$\mathrm{SFR_{Holes}} \approx 134\,\mathrm{SFR}\,(M_\odot \gtrapprox 8).$$

Утверждают, что хорошее согласие между SFR_holes и SFR_Ha или SFR_FUV, а значит фидбэк вносит доминирующий вклад в формирование оболочек HI.

# Chemical Abundances in Active Galaxies

Sophia R. Flury[1]★ and Edward C. Moran[2]
[1]Department of Astronomy, University of Massechusetts Amherst, Amherst, MA 01002, United States
[2]Department of Astronomy, Wesleyan University, Middletown, CT 06459, United States

Accepted 2020 May 29. Received 2020 May 20; in original form 2019 November 12



**ABSTRACT**

The Sloan Digital Sky Survey (SDSS) has proved to be a powerful resource for understanding the physical properties and chemical composition of star-forming galaxies in the local universe. The SDSS population of active galactic nuclei (AGN) remains as of yet less explored in this capacity. To extend the rigorous study of H II regions in the SDSS to AGN, we adapt methods for computing direct-method chemical abundances for application to the narrow-line regions (NLR) of AGN. By accounting for triply-ionized oxygen, we are able to more completely estimate the total oxygen abundance. We find a strong correlation between electron temperature and oxygen abundance due to collisional cooling by metals. Furthermore, we find that nitrogen and oxygen abundances in AGN are strongly correlated. From the metal-temperature relation and the coupling of nitrogen and oxygen abundances, we develop a new, empirically and physically motivated method for determining chemical abundances from the strong emission lines commonly employed in flux-ratio diagnostic diagrams (BPT diagrams). Our approach, which for AGN reduces to a single equation based on the BPT line ratios, consistently recovers direct-method abundances over a 1.5 dex range in oxygen abundance with an rms uncertainty of 0.18 dex. We have determined metallicities for thousands of AGN in the SDSS, and in the process have discovered an ionization-related discriminator for Seyfert and LINER galaxies.

**Key words:** ISM: abundances – galaxies: abundances – galaxies: active

## 1 INTRODUCTION

Spurred by revolutionary ideas about the nature of gaseous nebulae (e.g., Strömgren 1939), Menzel applied then-new ideas about quantum mechanics to emission-line phenomena to develop a working theory of nebular astrophysics, often in collaboration with Baker and Aller. This enabled the first empirical estimates of physical properties like electron temperature (Menzel & Aller 1941) and ionic abundances like $O^{+2}/H$ (Menzel et al. 1941) in gaseous nebulae. Seyfert, their contemporary, reported the discovery of a new class of emission-line objects in 1943 that later came to be known as active galactic nuclei (AGN). While Menzel's theand other Local Group galaxies; and (ii) AGN nebulae have a more complex ionization structure (e.g., Osterbrock & Ferland 2006, henceforth OF06). Sixteen years passed between the development of a method for the direct estimation of chemical abundances in the Orion Nebula (Aller & Liller 1959) and the first investigation of metallicity in an AGN (Osterbrock & Miller 1975). While Koski (1978) and Shuder & Osterbrock (1981) analyzed the physical properties of the gas in Seyfert nebulae, and Storchi-Bergmann & Pastoriza (1990) established the range of metallicities for a sample of AGN using photoionization models, it was not until Cruz-Gonzalez et al. (1991) that direct-method abundances (i.e., abundances determined using the electron temperature and


Как оценить относительное содержание тяжелых элементов в газе?
Отношение потоков рекомбинационных линий металлов и водорода
Нереально – линии металлов очень слабые
«Прямой» метод (Te-метод)
Нужен очень высокий S/N для детектирования [OIII]4363 и/или [NII]5755 + влияют вариации Te
Методы сильных линий (SEL)
Калибровка по HII областям
Можно использовать только для того класса объектов и в том диапазоне металличности, что и для опорных объектов
Калибровка по фотоионизационным моделям
Точность и применимость зависит от реалистичности модели и точности атомных данных

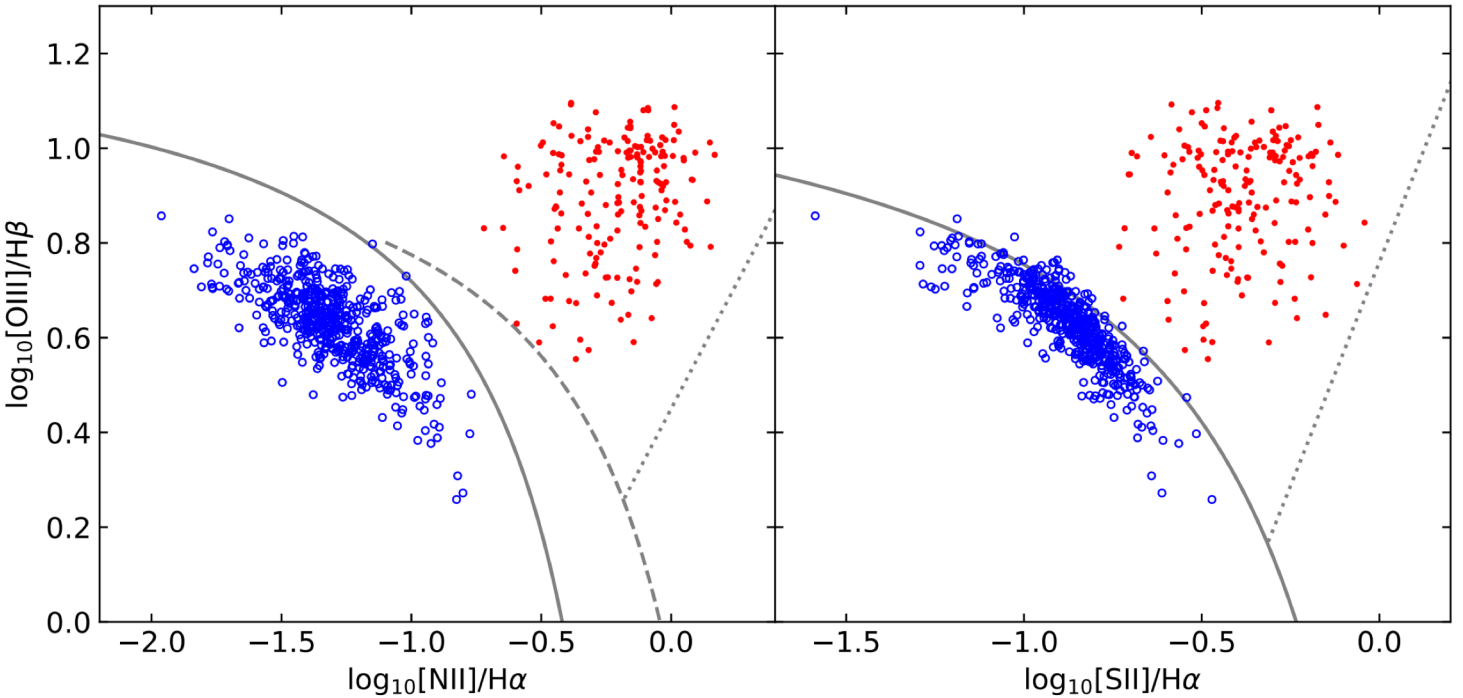


**Figure 1.** BPT diagnostic diagrams for our samples of AGN (filled red symbols) and H II galaxies (open blue symbols) from the SDSS DR8. The solid curves indicate the empirical demarcations between H II galaxies and AGN defined by Kauffmann et al. (2003) and Kewley et al. (2006). The dashed curve on the [N II]/H$\alpha$ plot represents the theoretical "maximum starburst" line from Kewley et al. (2001). In the AGN zones, empirical divisions between Seyfert galaxies and LINERs (Schawinski et al. 2007; Kewley et al. 2006) are indicated by dotted lines.

Используют данные SDSS DR8, точнее – опубликованные потоки в эмиссионных линиях после Protsmouth processing (Thomas et al. 2013)

Начальная выборка – 152322 HII и 8720 AGN

Выборка для использования Te-метода (нужны линии [OIII]4363, [OII]3727 с хорошим S/N) – 539 HII и 180 AGN, z~0.02

## 1) Считаем $n_e$ и $T_e$, используя PyNeb (Luridiana+ 2015).

Исходя из 5-уровневой модели атома, получаем

$$\frac{j\lambda6716}{j\lambda6731} = a_n \frac{1 + b_n\ n_e}{1 + c_n\ n_e} \qquad \frac{j\lambda4959 + j\lambda5007}{j\lambda4363} = \frac{a_T\ \exp\left(b_T\ T_e^{-1}\right)}{1 + c_T\ T_e^{-1/2}}$$

**Table 1.** Parameters for [S II] doublet ratio vs. electron density for a range of electron temperatures.

| $T_e$ ($10^4$ K) | $a_n$ | $b_n$ (cm$^3$) | $c_n$ (cm$^3$) |
|---|---|---|---|
| 0.5 | 1.471 | 6.710 | 2.259 |
| 1.0 | 1.450 | 4.725 | 1.591 |
| 1.5 | 1.431 | 3.854 | 1.298 |
| 2.0 | 1.417 | 3.326 | 1.122 |
| 2.5 | 1.406 | 2.967 | 1.001 |
| 3.0 | 1.396 | 2.700 | 0.909 |
| 3.5 | 1.391 | 2.483 | 0.837 |

**Table 2.** Parameters for [O III] doublet-auroral line ratio vs. electron temperature for a range of electron densities.

| $n_e$ (cm$^{-3}$) | $a_T$ | $b_T \times 10^4$ K | $c_T$ (K$^{1/2}$) |
|---|---|---|---|
| 10 | 7.995 | 3.331 | 8.937 |
| $10^2$ | 7.987 | 3.330 | 8.844 |
| $10^3$ | 7.964 | 3.330 | 8.970 |
| $10^4$ | 7.995 | 3.341 | 14.913 |

$$T_{e,[\mathrm{O\ II}]} = \left(\frac{6930}{T_{e,[\mathrm{O\ III}]}} + 2810\ \mathrm{K}^{-1}\right)^{-1}$$

from Pérez-Montero & Díaz (2003).

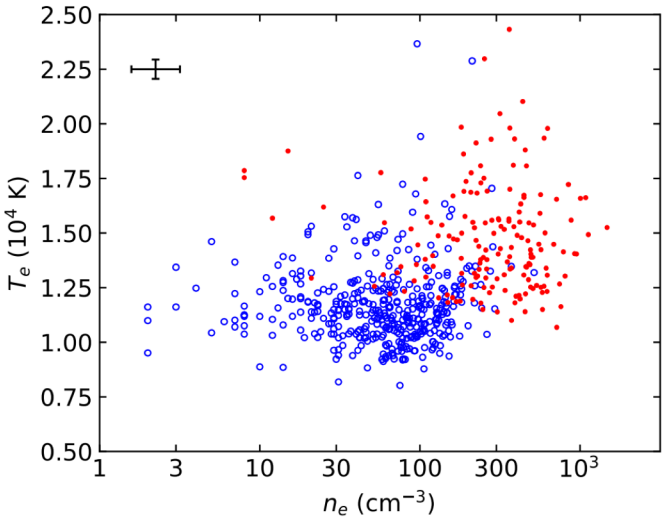


В отличии от обычного подхода, считают итеративно, используя «правильную» Te для расчета ne

2) **Считаем ионные относительные содержания кислорода (и азота)**

Предполагая 3-зонную модель туманности, получаем

$$\frac{O}{H} = \frac{O^+ + O^{+2} + O^{+3}}{H^+}.$$

Для запрещенных линий: $$j_\lambda = n_{\chi^i} n_e \varepsilon_\lambda(n_e, T_e) \frac{4\pi\lambda}{hc},$$

Для рекомбинационных линий: $$j_\lambda = n_{\chi^i} n_e \alpha_{eff} \frac{4\pi\lambda}{hc}$$

$$\frac{O^{+2}}{H^+} = \frac{(j_{4959} + j_{5007})\alpha_{4861}}{(\varepsilon_{4959} + \varepsilon_{5007})j_{4861}}. \qquad \frac{O^+}{H^+} = \frac{(j_{3726} + j_{3729})\alpha_{4861}}{(\varepsilon_{3726} + \varepsilon_{3729})j_{4861}}.$$

$$\frac{N^+}{O^+} = \frac{(j_{6548} + j_{6583})(\varepsilon_{3726} + \varepsilon_{3729})}{(j_{3726} + j_{3729})(\varepsilon_{6548} + \varepsilon_{6583})}. \quad = N/O$$

## 3) Коррекция за ненаблюдаемые стадии ионизации

$$\frac{O^{+3}}{O^{+} + O^{+2} + O^{+3}} \propto \frac{He^{+2}}{He^{+} + He^{+2}}$$

$$O^{+3} = 0.5 \frac{y}{1-y} \left(O^{+} + O^{+2}\right),$$

where $y = He^{+2}(He^{+} + He^{+2})^{-1}$.

*Для вычисления ICF – используем потоки в линиях HeI 5876 и HeII 4686*

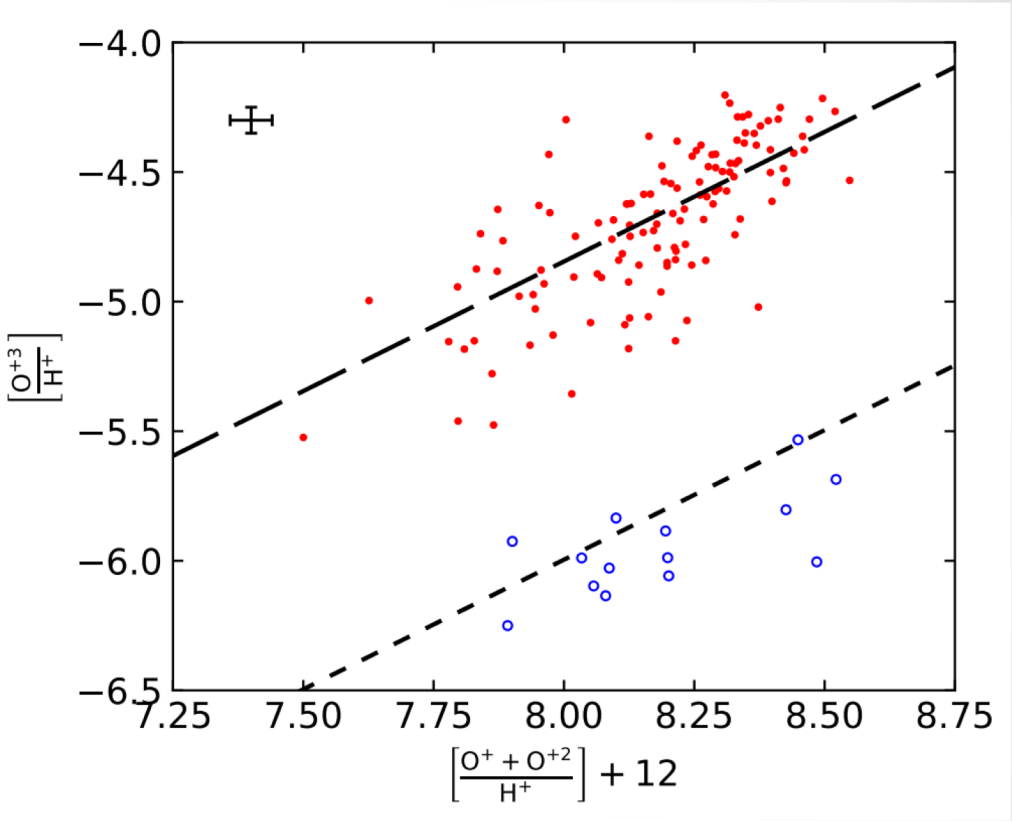


В случае AGN вклад $O^{+3}$ составляет порядка 12.5%, против ~1% в случае HII. Учет этой составляющей – очень важен и, вероятно, является причиной, почему до этого оценки, получаемые Te-методом для AGN считались неправильными (например, Dors et al. 2015)

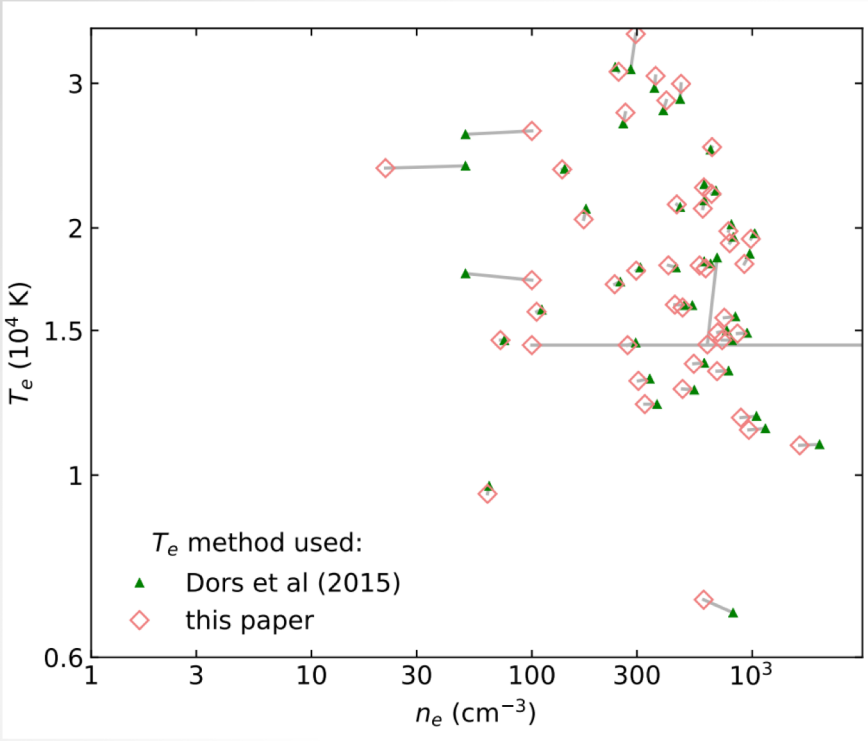


Сравнивают свои оценки с тем, что получено в работе Dors et al. (2015). Хорошее согласие Te и ne, но наблюдаются существенные различия в металличности.

Более точный расчет Te и ne уменьшает расхождение в O/H на ~0.05 dex

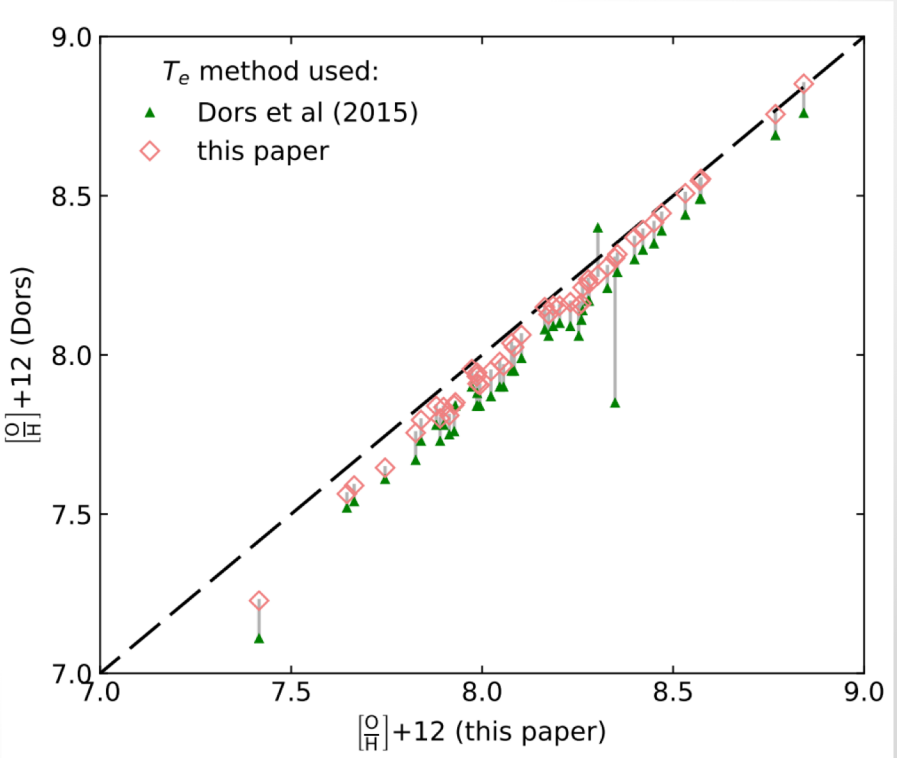


Сравнение с работой Dors+(2015) после коррекции их результатов за вклад $O^{+3}$

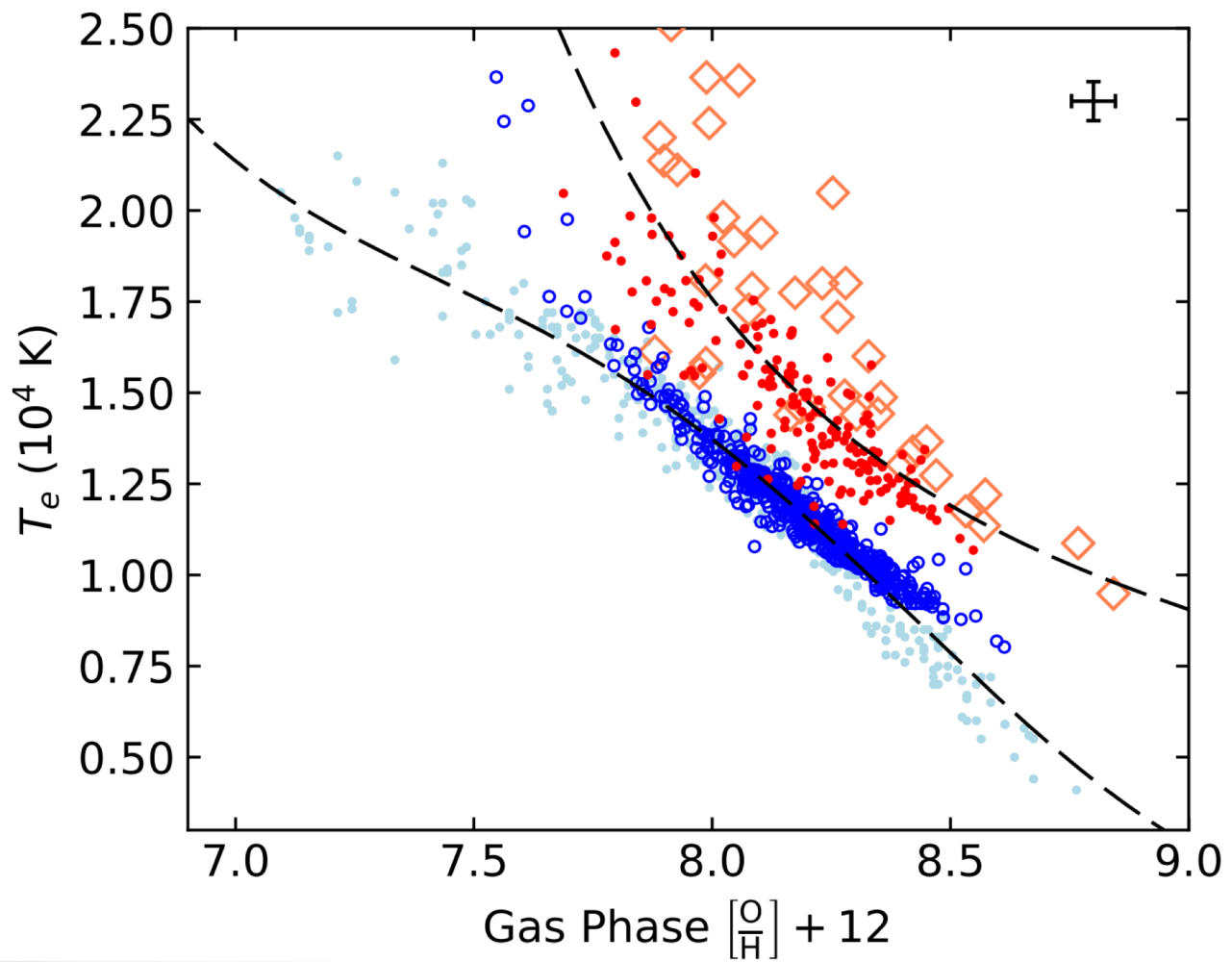


Более высокая Te в случае AGN увеличивает кинетическую энергию электронов, что приводит к уменьшению темпа рекомбинации $O^{+2}$ и к отсутствию сильного спада Te с ростом O/H

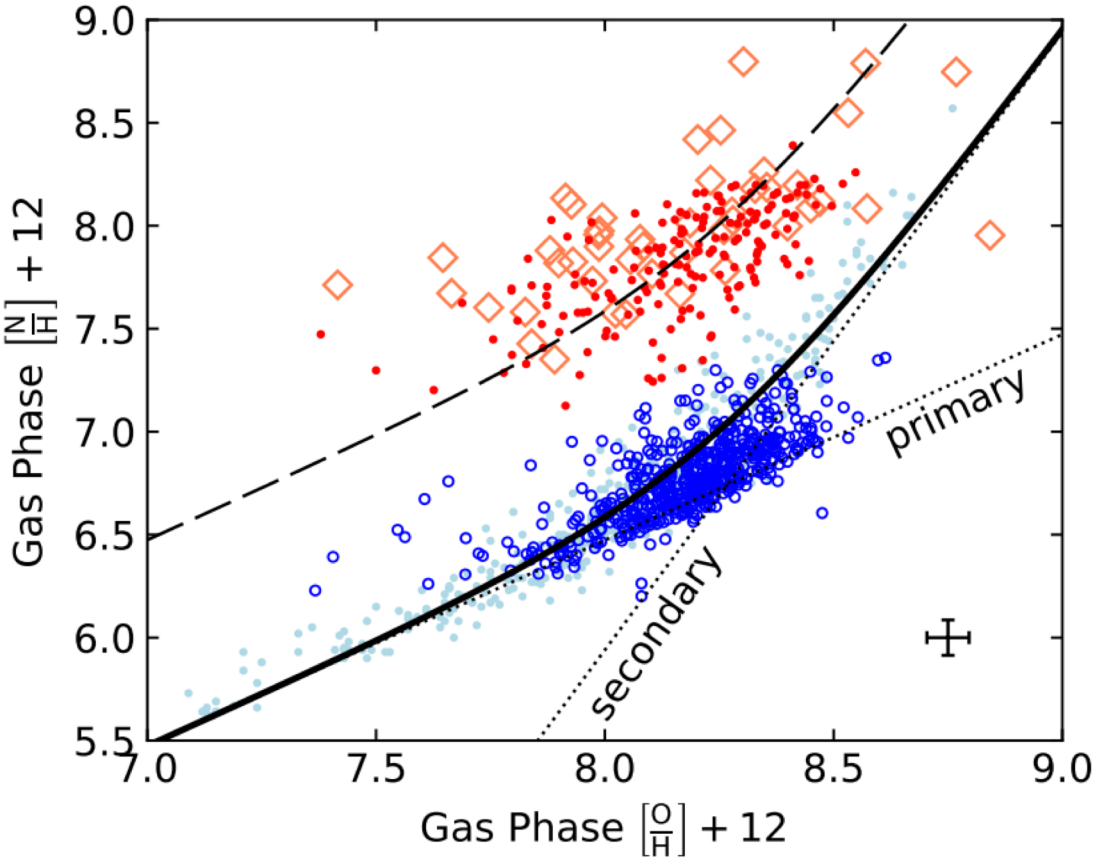


**Figure 7.** Nitrogen abundance vs. oxygen abundance for AGN and star-forming galaxies included in several different studies. Symbols as in Figure 6. The solid line represents our fit to the H II nitrogen production sequence. Dotted lines represent the primary and secondary nitrogen components of the relation. The dashed lines represents the H II nitrogen production relation shifted by 0.75 dex in [N/H] and 0.125 in [O/H] to match the observed AGN abundances.

В AGN – N/H систематически выше

# Строят сетку моделей для использования SEL

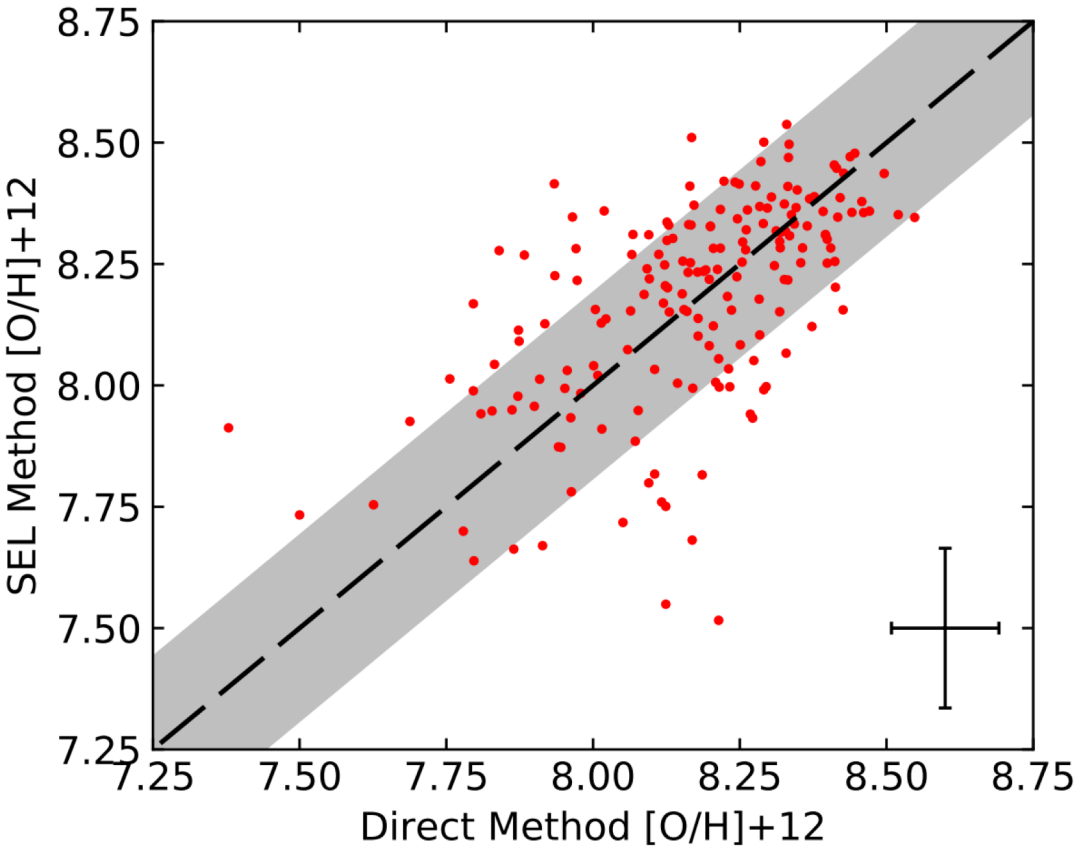


$$\frac{j_{\lambda 6583}}{j_{\lambda 6563}} = \frac{\mathrm{N}^+}{\mathrm{H}^+} \frac{\varepsilon_{\lambda 6583}(T_e, n_e)}{\alpha_{\lambda 6563}(T_e)}$$

$$\frac{j_{\lambda 5007}}{j_{\lambda 4861}} = \frac{\mathrm{O}^{+2}}{\mathrm{H}^+} \frac{\varepsilon_{\lambda 5007}(T_e, n_e)}{\alpha_{\lambda 4861}(T_e)}$$

$$\eta = \frac{\mathrm{O}^{+2}}{\mathrm{O}}, \qquad \zeta \approx \begin{cases} 0.01 & \text{H II} \\ 0.125 & \text{AGN} \end{cases}$$

which gives

$$\frac{\mathrm{O}^{+2}}{\mathrm{H}^+} = \eta \frac{\mathrm{O}}{\mathrm{H}}.$$

$$\begin{aligned} z = \; & 7.863 + 1.170x + 0.027y - 0.369x^2 \\ & +0.208y^2 - 0.406xy - 0.100x^3 \\ & +0.323y^3 + 0.354x^2y - 0.333xy^2 \end{aligned}$$

$$x = \log\ [\mathrm{N\,II}]/\mathrm{H}\alpha, \quad y = \log\ [\mathrm{O\,III}]/\mathrm{H}\beta,$$

$$\frac{j_{\lambda 6583}}{j_{\lambda 6563}} = (1 - \eta - \zeta) \frac{\mathrm{N}}{\mathrm{H}} \left(\frac{\mathrm{O}}{\mathrm{H}}\right) \frac{\varepsilon_{\lambda 6583}}{\alpha_{\lambda 6563}} (t_4(\mathrm{O/H}))$$

and

$$\frac{j_{\lambda 5007}}{j_{\lambda 4861}} = \eta \frac{\mathrm{O}}{\mathrm{H}} \frac{\varepsilon_{\lambda 5007}}{\alpha_{\lambda 4861}} (t_4(\mathrm{O/H}))$$

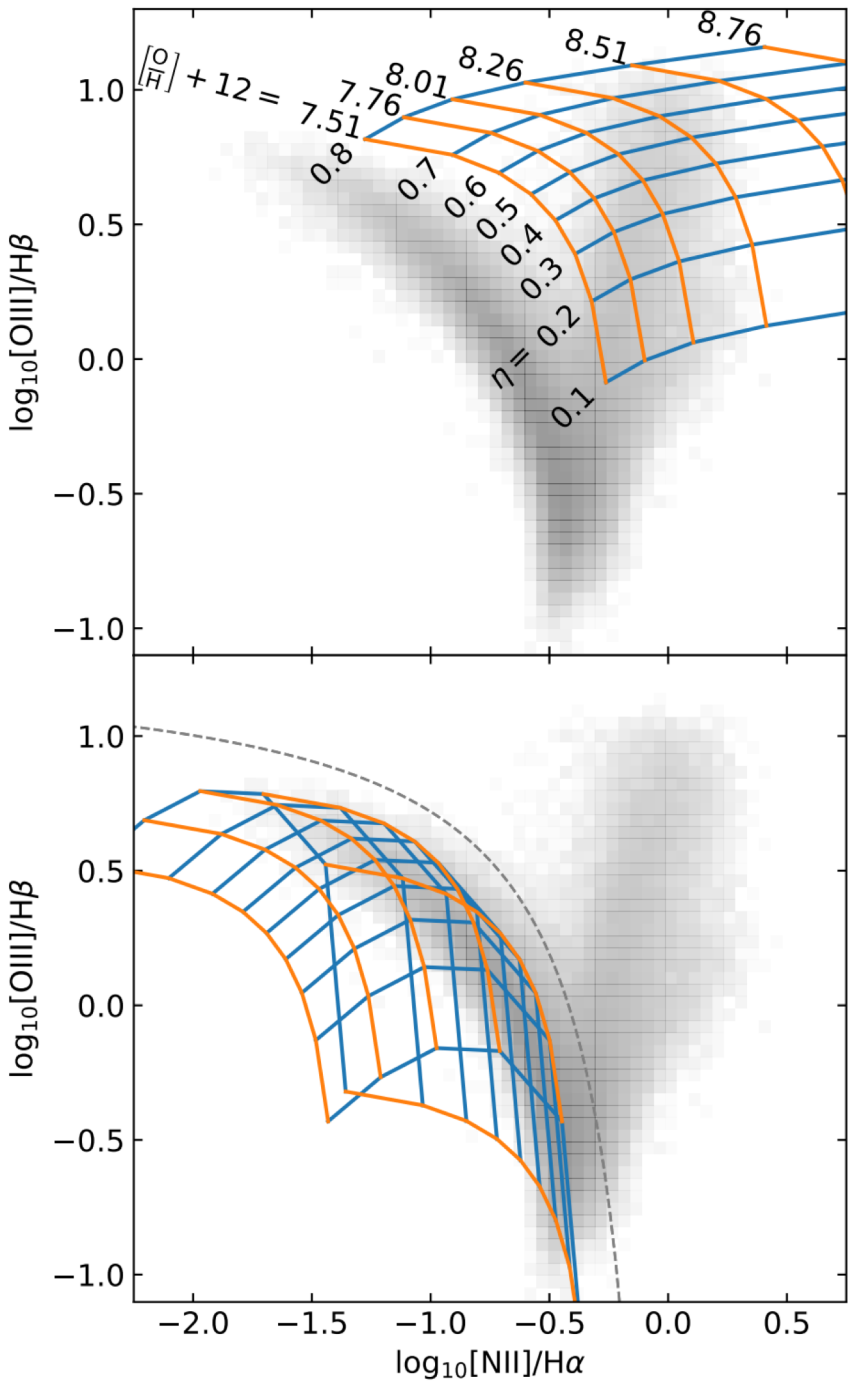


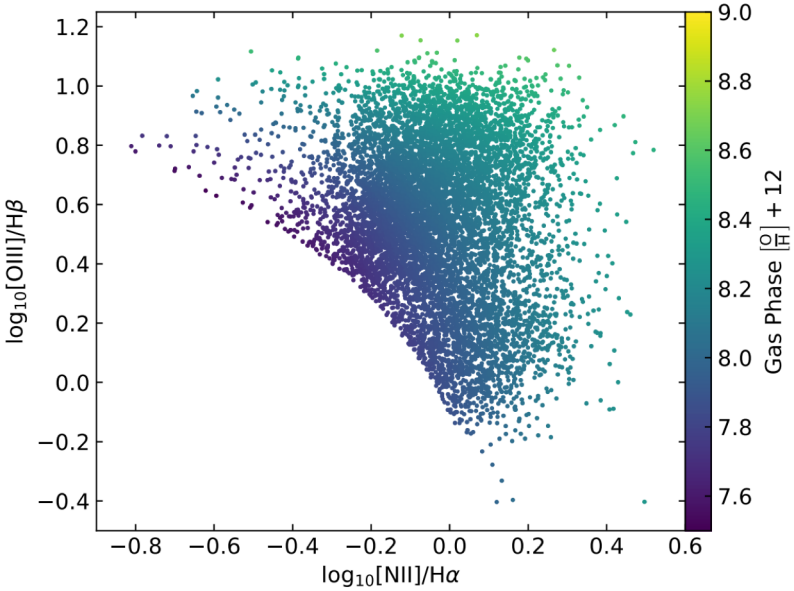


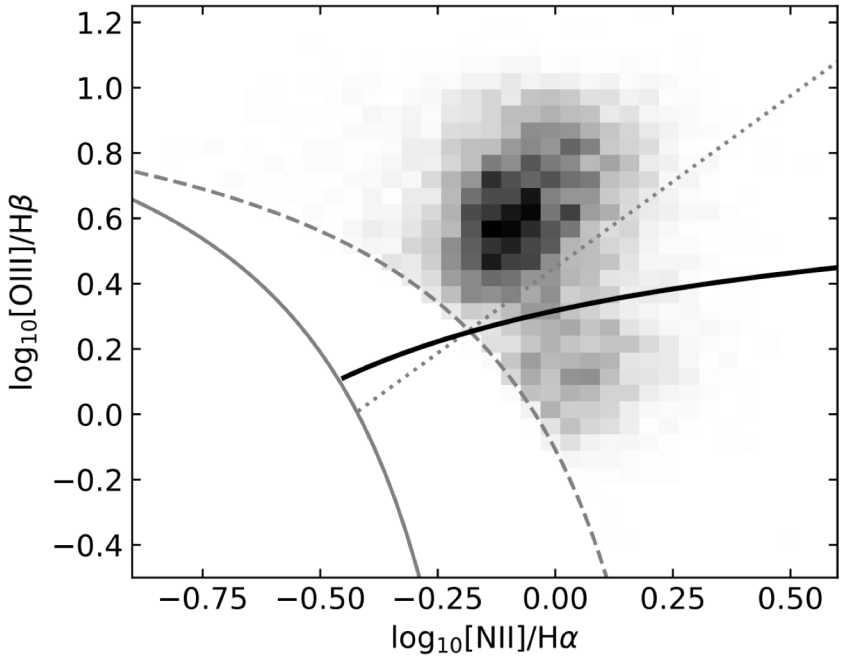


$$y = \frac{-0.628}{x + 1.417} + 0.753$$

$$\eta = 0.190$$